
Article:
Silva, L, Jackson, LP and Mound, J (2012) Assessing the importance and expression of the 6-year geomagnetic oscillation. Journal of Geophysical Research. Solid Earth, 117 (B10). ISSN: 2169-9313

https://doi.org/10.1029/2012JB009405

Assessing the importance and expression of the 6 year geomagnetic oscillation

L. Silva,[1] L. Jackson,[1] and J. Mound[1]

Received 26 April 2012; revised 9 August 2012; accepted 29 August 2012; published 9 October 2012.

[1] The first time derivative of residual length-of-day observations is known to contain a distinctive 6 year periodic oscillation. Here we theorize that through the flow accelerations at the top of the core the same periodicity should arise in the geomagnetic secular acceleration. We use the secular acceleration of the CHAOS-3 and CM4 geomagnetic field models to recover frequency spectra through both a traditional Fourier analysis and an empirical mode decomposition. We identify the 6 year periodic signal in the geomagnetic secular acceleration and characterize its spatial behavior. This signal seems to be closely related to recent geomagnetic jerks. We also identify a 2.5 year periodic signal in CHAOS-3 with unknown origin. This signal is strictly axially dipolar and is absent from other magnetic or geodetic time series.

Citation: Silva, L., L. Jackson, and J. Mound (2012), Assessing the importance and expression of the 6 year geomagnetic oscillation., *J. Geophys. Res.*, *117*, B10101, doi:10.1029/2012JB009405.

1. Introduction

[2] The residual length of day (LOD), after accounting for the variations in atmospheric angular momentum [*Ponsar et al.*, 2003], contains a broad range of periods but the high-frequency part of its spectrum features a strong signal with a period of approximately 6 years [*Abarca del Rio et al.*, 2000; *Mound and Buffett*, 2006]. This signal is thought to be the consequence of the interactions between the Earth's core and mantle [*Mound and Buffett*, 2006, 2007] and can be related to the fluid flow at the top of the core if this flow is assumed to be representative of the motions deeper inside the core [*Jault et al.*, 1988; *Jault and Le Mouël*, 1991; *Jackson et al.*, 1993]. Since the flow at the top of the core is responsible for the geomagnetic secular variation (SV), it is plausible to think that the 6 year periodic signal present in LOD should have a counterpart in the magnetic signal [*Gillet et al.*, 2010]. We show this to be the case provided that the time variations of the magnetic field are dominated by low frequencies (section 3).

[3] We use a time series of LOD (R. Holme, personal communication, 2010) to confirm the existence of this 6 year periodic signal exposed by *Abarca del Rio et al.* [2000]. This time series extends from 1962 to 2008 and has a sampling rate of 17 days. To emphasize the shorter periods we look at the first time derivative of LOD. We also compute frequency spectra of the secular acceleration (SA) provided by the CHAOS-3 [*Olsen et al.*, 2010] and CM4 [*Sabaka et al.*, 2004] models. CHAOS-3 represents Earth's main magnetic field between 1997 and 2010 with time-varying Gauss coefficients up to spherical harmonic degree and order 20. The time varying coefficients of the SV are expanded in terms of order 6 B splines, with a 6 month knot spacing. This 13 year long model has high spatiotemporal resolution and accuracy, making it ideal to study short time scale oscillations of the field. Although CHAOS-3 may be too short a time series to resolve signals with a period of the order of 6 years unequivocally, it allows us to consider whether they are a possible element of the solution. To account for the small length of the CHAOS-3 time series, we also analyze CM4 for periodic signals. CM4 represents the main magnetic field of the Earth for 42.5 years between 1960 and 2002.5. Coefficients of the SV are expanded in terms of cubic B splines up to spherical harmonic degree and order 13. A 42.5 year time span may allow for a much better assessment of periods up to 20 years with a Fourier analysis but a knot spacing of 2.5 years may not be ideal for the correct recovery of shorter periods.

[4] We take two different approaches to evaluate the Fourier spectrum of the SA. First, we take the frequency spectrum of the SA globally (see section 4.1). We then compare these results with the average of spectra taken at 44 locations (see section 5.1). To assess whether aliasing effects associated with the application of Fourier analysis on relatively short time series (i.e., CHAOS-3) contaminated our results, we also use an empirical mode decomposition (EMD) [*Huang et al.*, 1998; *Roberts et al.*, 2007; *Jackson and Mound*, 2010] of time series obtained from CHAOS-3 and CM4 at the above 44 locations. The procedure is described in section 4.2 and the corresponding results are shown in section 5.2.

[5] Finally, we present maps of the SA (section 5.3), filtered to the period range between 5 and 8 years at the core-mantle boundary (CMB), highlighting its spatial features.

[1]School of Earth and Environment, University of Leeds, Leeds, UK.

Corresponding author: L. Silva, School of Earth and Environment, University of Leeds, Leeds LS2 9JT, UK. (l.a.c.silva@leeds.ac.uk)

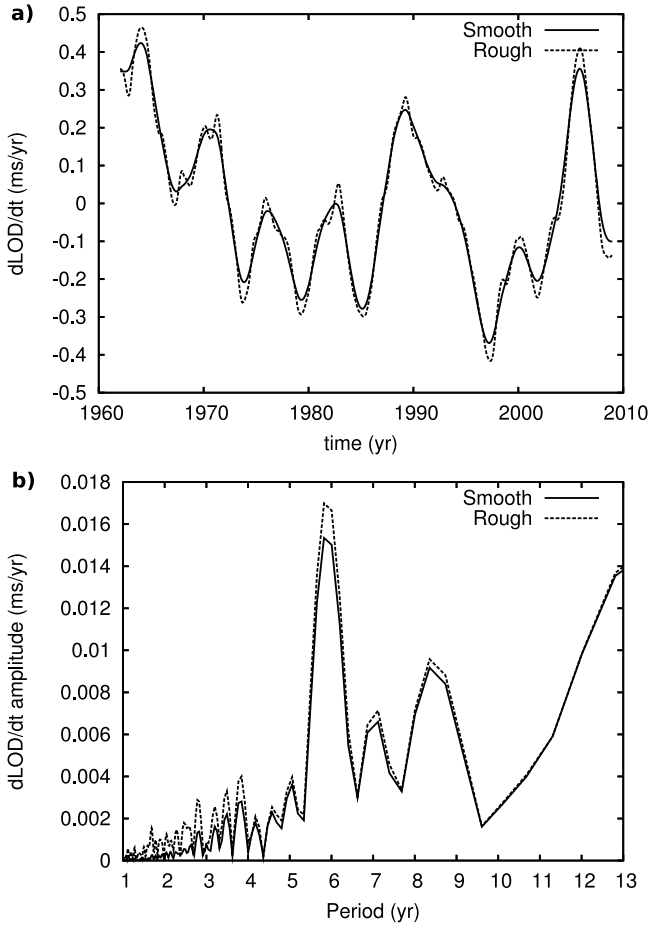

Figure 1. Filtered time series of dLOD/dt from *Holme* [2010]: (a) original signal and (b) frequency spectrum.

A general discussion of the results and the conclusions are presented in section 6.

2. Fourier Spectra of dLOD/dt

[6] We computed the discrete Fourier transform of a time series of dLOD/dt reported by *Holme and De Viron* [2005] and extended by *Holme* [2010]. This time series is a penalized least squares spline fit to the data after removal of atmospheric contributions and periodic annual and semiannual signals. *Holme* [2010] tested two penalizations for the spline fits resulting in "smooth" and "rough" curves. Figure 1a shows these signals as a function of time for both the smooth and rough cases. Figure 1b shows the amplitude of these signals as a function of the period of oscillation. Most of the power is restricted to periods above 5 years with a clear peak close to 6 years (as was also seen by *Mound and Buffett* [2006]). Considering the rough time series instead of the smooth one increases the energy of the short period noise and further emphasizes the 6 year signal.

3. Relation Between dLOD/dt, Flow Acceleration, and Secular Acceleration

[7] The fastest oscillations of dLOD/dt are thought to originate from mantle-atmosphere and mantle-ocean interactions. These contributions being corrected for, the remaining signal is thought to result from the interaction between the core and the mantle and reflect the changes in flow at the top of the core. The part of the SA generated by the flow acceleration at the top of the core should, therefore, evolve in a fashion coherent with that of the dLOD/dt.

[8] To investigate that relation, we start by describing the flow acceleration, $\dot{\vec{u}}$, at the top of the free stream, just below the CMB, which can be written in terms of surface vector spherical harmonics as

$$\dot{\vec{u}}(t) = \sum_{p=1}^{\infty}\sum_{q=0}^{p}\sum_{k=c,s}\left\{\dot{s}_p^{qk}(t)\vec{S}_p^{qk} + \dot{t}_p^{qk}(t)\vec{T}_p^{qk}\right\}. \quad (1)$$

Here, the $\vec{S}_p^{qk} = r_o\vec{\nabla}_{\mathrm{H}}\mathrm{Y}_p^{qk}$ are the poloidal and $\vec{T}_p^{qk} = r_o\vec{\nabla}_{\mathrm{H}}\times\left(\hat{r}\mathrm{Y}_p^{qk}\right)$ the toroidal elementary vectors of degree p and order q and either $k = c$ for cosine or $k = s$ for sine. r_o is the radius of the outer core and the $\mathrm{Y}_p^{qc/s}$ and $\mathrm{Y}_p^{qc/s}$ are Schmidt seminormalized spherical harmonics. $\vec{\nabla}_{\mathrm{H}}$ is the horizontal part of the del operator in spherical coordinates. Here, as in the remainder of this paper, dots over symbols represent a partial derivative with respect to time, of order equal to the number of dots.

[9] To first order, the pressure forces inside Earth's core are thought to be balanced by the Coriolis force. This balance of forces implies that zonal motions inside the core are invariant with respect to the direction along the axis of rotation of the mantle. It follows that such cylindrical motions are completely determined by the zonal motions at the surface of the core and, therefore, by the t_p^{0c} coefficients of the surface flow. *Jault et al.* [1988] and *Jault and Le Mouël* [1991] have shown that the axial angular momentum of the core relies only on the t_1^{0c} and t_3^{0c} coefficients of the flow. Conservation of the angular momentum of the whole Earth then implies that only these coefficients contribute to the changes in length of day [*Jault et al.*, 1988; *Jault and Le Mouël*, 1991; *Jackson et al.*, 1993]. The $\dot{t}_1^{0c}$ and $\dot{t}_3^{0c}$ coefficients of the flow acceleration are then trivially related to dLOD/dt through

$$dLOD/dt = \frac{(T_0)^2}{2\pi}\frac{I_c}{I_c + I_m}\left(\dot{t}_1^{0c} + \frac{12}{7}\dot{t}_3^{0c}\right), \quad (2)$$

where I_c and I_m are the moments of inertia of the core and mantle, respectively and $(T_0)^2/(2\pi) \times I_c/(I_c + I_m)$ equals 1.138×10^3 ms^2. The coefficients of the flow acceleration, $\dot{t}_1^{0c}$ and $\dot{t}_3^{0c}$ are given in yr^{-2} and the standard length of day is $T_0 = 8.64 \times 10^7$ ms. To obtain a dLOD/dt in ms/yr, we must perform a reduction amounting to dividing the result by the number of milliseconds in a year (3.156×10^{10} ms/yr).

[10] The flow acceleration at the top of the core also takes part in generating the SA. The first time derivative of the radial, frozen-flux induction equation

$$\ddot{\mathrm{B}}_r = -\vec{\nabla}_{\mathrm{H}}\cdot\left(\dot{\vec{u}}\mathrm{B}_r\right) - \vec{\nabla}_{\mathrm{H}}\cdot\left(\vec{u}\dot{\mathrm{B}}_r\right), \quad (3)$$

relates the flow and the flow acceleration to the geomagnetic field and its evolution with time. It indicates that the flow advects some of the SV to produce some SA but also that the

Table 1. Values of the Interaction Integrals (Equation (8)) for the First Five Degrees of the SA and Main Field[a]

i	j	n	$I1sc_{ni}^{jj}$	$I3sc_{ni}^{jj}$
1	1	1	0.70710678	0
2	1	2	0.23570226	0.40406102
2	2	2	0.47140452	−0.20203051
3	1	1	0	0.74230749
3	1	3	0.11785113	0.23570226
3	2	3	0.23570226	0.23570226
3	3	3	0.35355339	−0.23570226
4	1	2	0	0.30737963
4	2	2	0	0.43470044
4	1	4	0.07071068	0.14876792
4	2	4	0.14142136	0.21488700
4	3	4	0.21213203	0.11570838
4	4	4	0.28284271	−0.23141676
5	1	3	0	0.16939909
5	2	3	0	0.28345889
5	3	3	0	0.28345889
5	1	5	0.04714045	0.10153328
5	2	5	0.09428090	0.16680468
5	3	5	0.14142136	0.15955230
5	4	5	0.18856181	0.04351426
5	5	5	0.23570226	−0.21757132

[a]Here i and n are the degrees of the SA and main field, respectively, and j is the common order.

field itself interacts with the flow acceleration. The second term on the right hand side of equation (3) is known to be negligible with respect to the first (2% to 10% of the total SA depending on the degree and epoch) [*Maus et al.*, 2008; *Lesur et al.*, 2010; *Silva and Hulot*, 2012]. The SA can, therefore, be well approximated by the interactions between the flow acceleration and the main geomagnetic field

$$\ddot{\mathrm{B}}_r \approx -\vec{\nabla}_{\mathrm{H}} \cdot \left(\vec{u}\mathrm{B}_r\right). \tag{4}$$

[11] Equations (2) and (4) tell us that only the $\dot{t}_1^{0c}$ and $\dot{t}_3^{0c}$ coefficients of the flow acceleration can relate to both dLOD/dt and SA. To understand this relation, we start by expanding equation (4) in terms of spherical harmonics using the standard decomposition of the radial component of the field and SA:

$$\mathrm{B}_r = \sum_{n=1}^{\infty}\sum_{m=0}^{n}(n+1)\left(\frac{a}{r}\right)^{(n+2)}\left(g_n^m \mathrm{Y}_n^{mc} + h_n^m \mathrm{Y}_n^{ms}\right) \tag{5}$$

$$\ddot{\mathrm{B}}_r = \sum_{i=1}^{\infty}\sum_{j=0}^{i}(i+1)\left(\frac{a}{r}\right)^{(i+2)}\left(\ddot{g}_i^j \mathrm{Y}_i^{jc} + \ddot{h}_i^j \mathrm{Y}_i^{js}\right). \tag{6}$$

We can now substitute equations (1), (5), and (6) at the CMB into equation (4) to give

$$\begin{aligned}\sum_{i=1}^{\infty}\sum_{j=0}^{i}(i+1)\left(\frac{a}{r_o}\right)^{(i+2)}&\left(\ddot{g}_i^j \mathrm{Y}_i^{jc} + \ddot{h}_i^j \mathrm{Y}_i^{js}\right)\\ \approx -\vec{\nabla}_{\mathrm{H}} \cdot \sum_{n=1}^{\infty}\sum_{m=0}^{n}(n+1)&\left(\frac{a}{r_o}\right)^{(n+2)}\sum_{p=1}^{\infty}\sum_{q=0}^{p}\sum_{k=c,s}\Big[\left(\dot{s}_p^{qk}\vec{S}_p^{qk} + \dot{t}_p^{qk}\vec{T}_p^{qk}\right)\\ &\cdot\left(g_n^m \mathrm{Y}_n^{mc} + h_n^m \mathrm{Y}_n^{ms}\right)\Big].\end{aligned} \tag{7}$$

[12] The contribution of the toroidal zonal flow acceleration coefficients $\dot{t}_1^{0c}$ and $\dot{t}_3^{0c}$ to the secular acceleration is then given by

$$\ddot{\mathcal{G}}_i^j \approx \sum_{n=1}^{\infty}\frac{(2i+1)}{4\pi}\frac{n+1}{i+1}\left(\frac{a}{r_o}\right)^{(n-i)}\sum_{m=0}^{n}\left\{\dot{t}_1^{0c}h_n^m I1sc_{ni}^{mj} + \dot{t}_3^{0c}h_n^m I3sc_{ni}^{mj}\right\} \tag{8}$$

$$\ddot{\mathcal{H}}_i^j \approx \sum_{n=1}^{\infty}\frac{(2i+1)}{4\pi}\frac{n+1}{i+1}\left(\frac{a}{r_o}\right)^{(n-i)}\sum_{m=0}^{n}\left\{\dot{t}_1^{0c}g_n^m I1cs_{ni}^{mj} + \dot{t}_3^{0c}g_n^m I3cs_{ni}^{mj}\right\}, \tag{9}$$

with

$$I1sc_{ni}^{mj} = \iint_S \vec{T}_1^0 \cdot \left(\vec{\nabla}_{\mathrm{H}}\mathrm{Y}_n^{ms}\right)\mathrm{Y}_i^{jc}d\Omega, \tag{10}$$

$$I3sc_{ni}^{mj} = \iint_S \vec{T}_3^0 \cdot \left(\vec{\nabla}_{\mathrm{H}}\mathrm{Y}_n^{ms}\right)\mathrm{Y}_i^{jc}d\Omega, \tag{11}$$

$$I1cs_{ni}^{mj} = \iint_S \vec{T}_1^0 \cdot \left(\vec{\nabla}_{\mathrm{H}}\mathrm{Y}_n^{mc}\right)\mathrm{Y}_i^{js}d\Omega, \tag{12}$$

$$I3cs_{ni}^{mj} = \iint_S \vec{T}_3^0 \cdot \left(\vec{\nabla}_{\mathrm{H}}\mathrm{Y}_n^{mc}\right)\mathrm{Y}_i^{js}d\Omega, \tag{13}$$

where results obtained by equation (16) of *Hulot et al.* [1992] were used to eliminate the integrals that evaluate to zero. The integrals $I1sc_{ni}^{jj}$, $I3sc_{ni}^{jj}$, $I1cs_{ni}^{mj}$ and $I3cs_{ni}^{mj}$ will only evaluate to a nonzero value if the field and SA coefficients are of the same nonzero spherical harmonic order, $m = j$. These integrals have been shown to be bounded and convergent for large values of i and n [*Hulot et al.*, 1992]. Values of $I1sc_{ni}^{jj}$ and $I3sc_{ni}^{jj}$ up to degree and order 5 are shown in Table 1. For brevity, we will focus on the $\ddot{\mathcal{G}}_i^j$, but a similar analysis can be performed for the $\ddot{\mathcal{H}}_i^j$.

[13] We applied a Fourier transform to equation (8) so that a given oscillation frequency of the SA can be associated with the oscillation frequencies of both the field and flow acceleration. This leads to

$$\begin{aligned}\tilde{\ddot{\mathcal{G}}}_i^j(\omega) \approx \sum_{n=1}^{\infty}\frac{(2i+1)}{4\pi}\frac{n+1}{i+1}\left(\frac{a}{c}\right)^{(n-i)}&\int \tilde{h}_n^j(\omega-\omega_u)\Big(\tilde{\dot{t}}_1^0(\omega_u)I1sc_{ni}^{jj}\\ &+ \tilde{\dot{t}}_3^0(\omega_u)I3sc_{ni}^{jj}\Big)\mathrm{d}\omega_u,\end{aligned} \tag{14}$$

where ω_u is the frequency of the flow and dLOD/dt and $\sim$ over symbols represents the Fourier transform of the quantity given by the symbol.

[14] The integral in equation (14) is only appreciable for those values of ω that make $h_n^j(\omega - \omega_u)$ appreciable. *McLeod* [1996] has shown that most of the energy of the field is in its low-frequency component. This is especially true for the large spatial scales of the field, which dominate even at the CMB, making $\tilde{h}_n^j(\omega - \omega_u)$ only appreciable when ω_u is close to ω. Therefore, the SA generated by interactions between the field and the $\dot{t}_1^{0c}$ and $\dot{t}_3^{0c}$ coefficients of the flow

acceleration should oscillate in a manner close to that of the dLOD/dt; deviations from an exact match and dispersion result from the fact that the field has some energy on frequencies higher than zero.

[15] The above exercise serves to show that the dominant frequencies present in dLOD/dt also gives a contribution to the SA. This contribution to the SA may be generated by the very large scale toroidal zonal flow acceleration interacting with the nonzonal field if the latter is steady on short time scales, a situation that seems to be applicable to the Earth. Should the field vary more quickly at the CMB, the spectrum of its SA would bear much less resemblance to that of dLOD/dt.

4. Frequency Analysis of the Secular Acceleration

4.1. Fourier Approach

[16] The frequency spectrum of the secular acceleration can be computed in a number of ways. It is therefore useful to define this spectrum. The Fourier transform of the radial component of the main field's secular acceleration can be written as (recall equation (5))

$$\tilde{\ddot{\mathrm{B}}}_r = \sum_{i=1}^{\infty}\sum_{j=0}^{i}(i+1)\left(\frac{a}{r}\right)^{(i+2)}\left(\tilde{\ddot{g}}_i^j(\omega)\mathrm{Y}_i^{jc} + \tilde{\ddot{h}}_i^j(\omega)\mathrm{Y}_i^{js},\right) \qquad (15)$$

where $\tilde{\ddot{g}}_i^j(\omega)$ and $\tilde{\ddot{h}}_i^j(\omega)$ are the Fourier transforms of the second time derivatives of the Gauss coefficients, $\ddot{g}_i^j(t)$ and $\ddot{h}_i^j(t)$.

4.1.1. Global Analysis

[17] $\tilde{\ddot{\mathrm{B}}}_r$ is a complicated quantity; its representation in space is difficult to visualize and interpret. Using the squared amplitude of $\tilde{\ddot{\mathrm{B}}}_r$ is still not satisfactory as it requires a series of map representations, one for each recovered frequency. We thus define the frequency spectrum of radial SA as the surface integral of the squared amplitude of equation (15). We can explicitly write this quantity as

$$\int |\tilde{\ddot{\mathrm{B}}}_r|^2 \mathrm{d}\Omega = \sum_{i=1}^{\infty}\sum_{l=1}^{\infty}(i+1)(l+1)\left(\frac{a}{r}\right)^{(l+i+4)}\sum_{j=0}^{i}\sum_{k=0}^{l} \cdot\left[\tilde{\ddot{g}}_i^{j*}(\omega)\tilde{\ddot{g}}_l^{k}(\omega)\int \mathrm{Y}_i^{jc}\mathrm{Y}_l^{kc}\mathrm{d}\Omega + \tilde{\ddot{h}}_i^{j*}(\omega)\tilde{\ddot{h}}_l^{k}(\omega) \cdot\int \mathrm{Y}_i^{js}\mathrm{Y}_l^{ks}\mathrm{d}\Omega\right], \qquad (16)$$

where we used the orthogonality conditions for the parity of spherical harmonics to make the separation between even and odd coefficients [*Abramowitz and Stegun*, 1964]. An asterisk denotes the complex conjugate of a complex quantity. Evaluating the integrals in equation (16) and summing over k and l leads to the desired expression for the spectrum $f(\omega)$:

$$f(\omega) = \frac{1}{4\pi}\int |\tilde{\ddot{\mathrm{B}}}_r|^2 \mathrm{d}\Omega = \sum_{i=1}^{N}\frac{(i+1)^2}{2i+1}\left(\frac{a}{r}\right)^{2(i+2)}\sum_{j=0}^{n}\left(|\tilde{\ddot{g}}_i^j(\omega)|^2 + |\tilde{\ddot{h}}_i^j(\omega)|^2\right). \qquad (17)$$

Equation (17) is the form used in the numerical implementation of the global spectrum. Calculations were performed for fixed radius, $r = a = 6371$ km (the Earth's surface).

4.1.2. Localized Analysis

[18] An alternative way of computing the frequency spectrum of the geomagnetic SA is to sample it at point locations over the surface of the Earth and then average those estimates. We use 10 equally spaced locations around the equator, 20 at midlatitudes (10 at 30°N, and 10 at 30°S), 12 at high latitudes (6 at 60°N and 6 at 60°S), and one at each of the poles. For each location the frequency spectrum is computed by taking the discrete Fourier transform (DFT) of the corresponding time series. In all cases, a best fit linear trend was first subtracted from the data. A cosine tapper was then applied and the data were padded with zeros up to four times its original length before computing DFTs. Making these changes does not greatly influence the final result but allows for a better resolution around the region of interest in frequency space.

4.2. Empirical Mode Decomposition Approach

[19] Although the Fourier approach is effective in finding the periodic components of a given signal, it does not cope well with periodic signals whose amplitudes vary with time. Furthermore, spurious periodicities and dispersion can arise from Fourier analysis if periods of similar length to the time series exist. In such cases empirical mode decomposition (EMD) can be used to decompose the series into a number of simple oscillations. The method, first outlined by *Huang et al.* [1998] and reviewed by *Huang and Wu* [2008], has been used in a variety of contexts including the study of periodicities of the geomagnetic field [e.g., *Roberts et al.*, 2007; *Jackson and Mound*, 2010].

[20] EMD is an analysis method which decomposes a time series into a set of quasiperiodic signals (intrinsic mode functions, IMF) and a residual. The sum of all the IMFs and the residual returns the original series. The IMFs are bounded, quasiperiodic functions with zero mean. When a periodicity exists, their autocorrelation function has semiregularly spaced maxima and minima that exceed a 95% confidence interval. The first minimum corresponds to half period ($p/2$), the first maximum to p, the second minimum to $3p/2$ and so on [*Roberts et al.*, 2007].

5. Results

5.1. Fourier Spectra of the Secular Acceleration

[21] Fourier spectra of the SA are shown in Figure 2. Thin light gray lines represent the spectra at the specified locations, while thick dark gray lines represent their average. Black dashed lines show the output of equation (17). It is clear that the spectral content varies quite significantly with the location at Earth's surface. Nevertheless, on average, the local and global methods seem to agree on the dominant periods of the signal.

[22] For CM4 (Figure 2a), a peak at around 5.5 years and another at roughly 7.5 years can be seen. However, the clear 6 year peak present in the dLOD/dt spectrum (Figure 1) corresponds here to a trough. We explain this by the fact that the 6 year signal has a time-dependent amplitude causing a splitting of the energy into two peaks, one with energy at

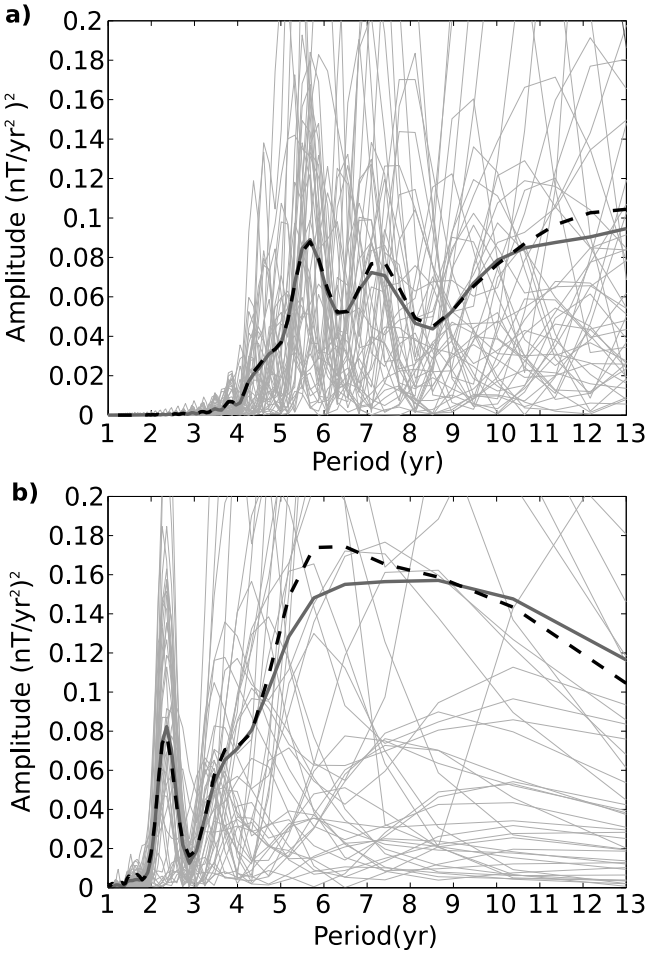

Figure 2. Frequency spectra of the secular acceleration for periods up to 13 years in (a) CM4 and (b) CHAOS-3. Thin gray lines are the frequency spectra for each location. Their average is shown by the thick dark gray line. The spectrum computed according to equation (17) is shown as a black dashed line.

shorter periods and the other with energy at longer periods. In fact, the periods are so close that they can be interpreted as the components of a beat. Using the periods of 5.5 and 7.5 years as the period of two interfering waves, the resulting beat would have a period of approximately 6.35 years and an envelope with a period of 41.25 years. In the next section we will see that this is indeed the case by analyzing the EMD decomposition of the signal. For periods above 8 years we can see a large energy dispersion which we do not try to interpret other than that it may contain the signature of the spectral timescale proposed by *Holme et al.* [2011].

[23] CHAOS-3 (Figure 2b), on the other hand, shows a clear and isolated peak at 2.5 years, with a large dispersion of the remaining energy at periods between 4 and 13 years. The highest energy seems, nevertheless, to be centered around a period of 6 years. Note that the amplitude of the average is an indication of how many locations registered a given frequency and not only the amplitude of the signal at that particular frequency. This will be made clearer with the EMD decomposition.

[24] To better understand the spatial composition of these features, we split the global Fourier spectrum of the CHAOS-3 model into terms of the same spherical harmonic degree (Figure 3a) and terms of the same spherical harmonic order (Figure 3b). The 6 year signal seems to be composed mostly by nonzonal terms. It is dominated by the coefficients of spherical harmonic degree 1 and 3 and of order 1. Such a signal can easily be generated by the toroidal zonal terms of the flow acceleration. Recalling Table 1, the degree 1 ($i = 1$), 6 year periodic signal is dominantly generated by $\dot{t}_1^{0c}$ (high values of $I1sc_{ni}^{jj}$) and the degree 3 ($i = 3$), by $\dot{t}_3^{0c}$ (high values of $I3sc_{ni}^{jj}$). Which of $\dot{t}_1^{0c}$ or $\dot{t}_3^{0c}$ dominates the budget for dLOD/dt is, therefore, linked to which of $\ddot{\mathcal{G}}_1^0$ ($\ddot{\mathcal{H}}_1^0$) or $\ddot{\mathcal{G}}_3^0$ ($\ddot{\mathcal{H}}_3^0$) dominate the SA at each instant. This separation may be used in the future to assess whether and which different processes contribute to both the generation of the secular acceleration and dLOD/dt.

[25] The 2.5 year signal in CHAOS-3, on the other hand, seems to result from an oscillation of the axial dipole ($i = 1$ and $j = 0$, see Figure 3). It has also been seen at observatory locations distributed worldwide [*Ladynin and Popova*, 2008] but no definite origin has been found for this signal.

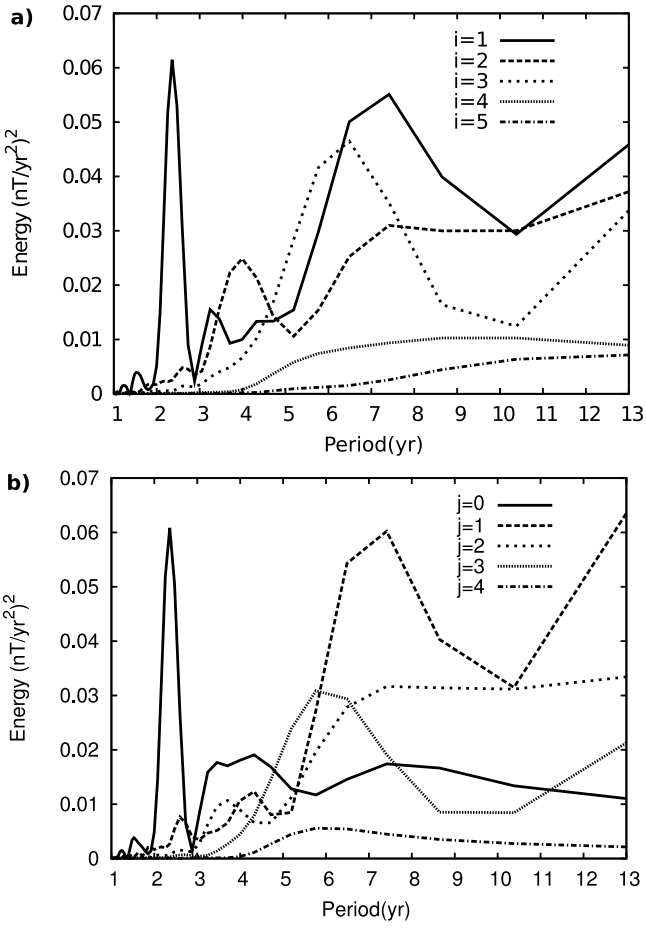

Figure 3. Frequency spectra of the secular acceleration from CHAOS-3. (a) Only the summation was carried over the order j in equation (16), each line corresponding to a degree i. (b) The summation was carried over the degree i, each line corresponding to an order j.

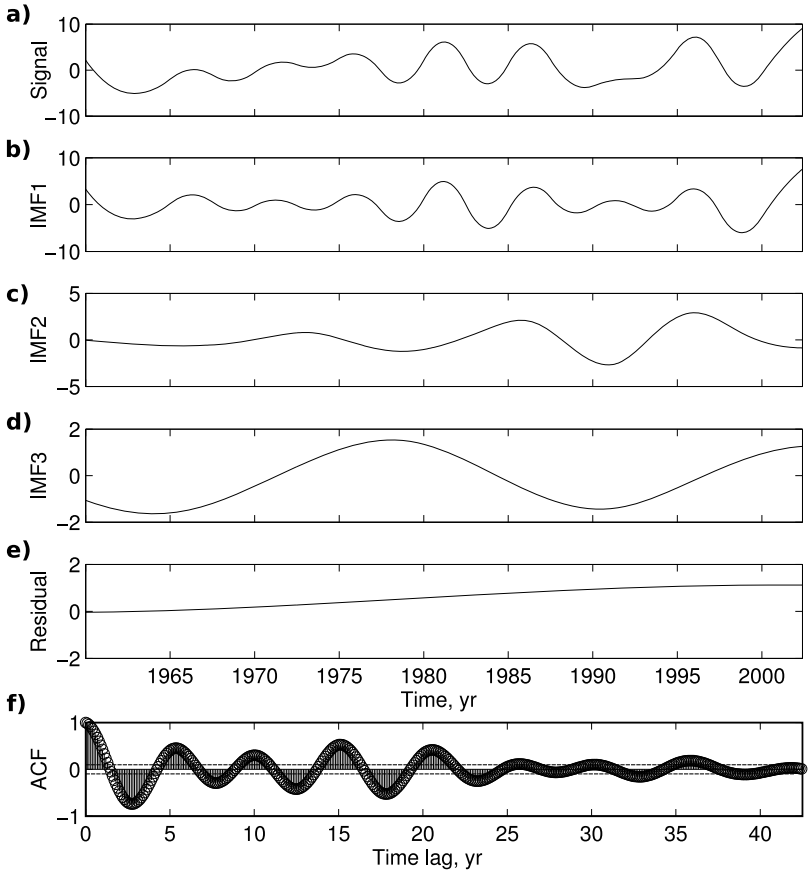

Figure 4. Empirical mode decomposition of a time series extracted from CM4 at position 60°N, 18°E. (a) The original signal. (b) First, (c) second, and (d) third IMFs. (e) The residual after the decomposition. (f) The autocorrelation function of IMF 1. Black horizontal lines in Figure 4f bound the 95% confidence interval.

At the CMB, an SA with $i = 1$ and $j = 0$ cannot be generated by the interactions of the field with the toroidal zonal flow acceleration (see equation (14) and Table 1) responsible for the changes in LOD, but can be the result of flow accelerations contributing to changes in pressure at the CMB [e.g., *Chulliat and Hulot*, 2000]. If these changes in pressure result in torques that are not aligned with the axis of rotation they may contribute to changes in the orientation of the Earth's rotation axis (the Earth orientation parameters, EOP) [*Hinderer et al.*, 1987, 1990; *Greff-Lefftz and Legros*, 1995; *Hide et al.*, 1996; *Hulot et al.*, 1996], although this signal should be small. A 2.5 year periodic signature of this process is, however, not present in the EOP data [see, e.g., *Gibert and Le Mouël*, 2008], rejecting the above hypothesis. This signal may either be of external (or induced) origin [*Wardinski*, 2005] or a consequence of the methods used to construct the CHAOS-3 model.

5.2. EMD Analysis of the SA

[26] We applied the EMD method to time series derived from both CM4 and CHAOS-3 for the 44 locations described above. Figure 4 shows the result of performing EMD upon an example time series extracted from CM4 at a point 60°N, 18°E. The same analysis was repeated for all time series obtained from both CM4 and CHAOS-3.

[27] Note that a given IMF does not strictly correspond to one given frequency. A certain frequency may even be present in two distinct IMFs although only at different times. Furthermore, for two different signals, a given IMF may correspond to totally different oscillations. This is the case for the IMFs of time series obtained at different locations. In this respect, grouping data by frequency rather than by IMF is a better choice (see Figure 5). Figure 5 shows the number of locations that registered a period within 1 year bins for both CM4 and CHAOS-3. The first bin in each panel represents signals with periods between 0 and 1 year.

[28] For CM4 (Figure 5a), a very large number of observatories register signals with a period between 5 and 7 years. Figure 4b shows that typical IMFs vary in amplitude over time but have a rather constant period, justifying the spectral splitting seen in the previous section. Periods between 11 and 13 years are also observed at a smaller number of locations. This latter signal is dominated by order 1 components as was the case for CHAOS-3 (see Figure 3b) which excludes a contamination from the solar cycle. This signal may, however, be a manifestation of the spectral timescale proposed by *Holme et al.* [2011]. We thus validate the spectra obtained with the Fourier methods, where energy was found at periods of 5.5 and 7.5 years followed by a spectral gap at 8.5 years and energy dispersion for periods above 10 years.

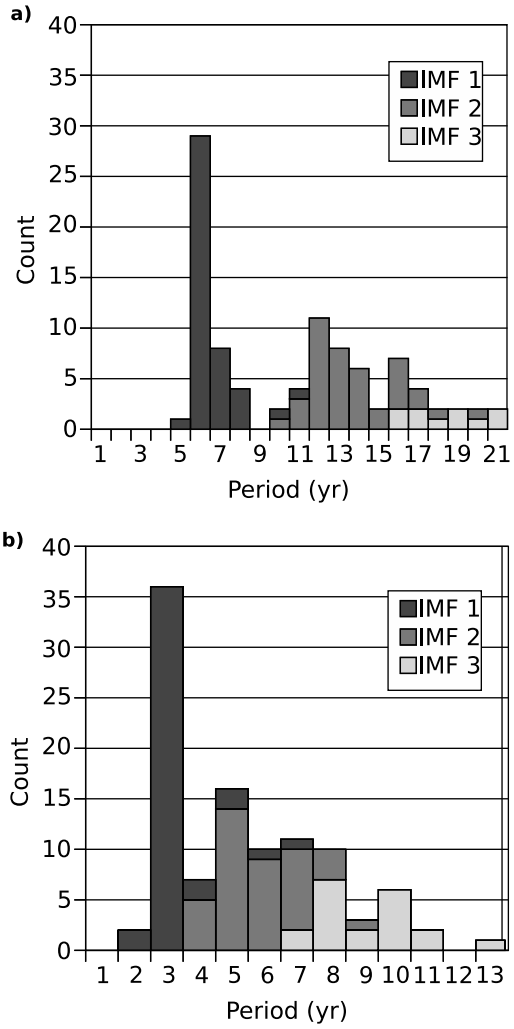

Figure 5. Number of locations reporting SA with period within each 1 year bin. The first bin represents periods between 0 and 1 year. Shades of gray represent results obtained for different IMFs. (a) Results from CM4 and (b) results from CHAOS-3.

[29] For CHAOS-3 (Figure 5b), a signal with periods between 2 and 3 years is registered at a large number of locations, validating the result of the Fourier analysis where this signal was characterized as an oscillation of the axially dipolar part of the SA. For the remaining period bins, the observatory count is nearly normally distributed around the 6 to 7 year bin with a predominance of signals with a period between 4 and 5 years. The longer period signals that make for a large contribution in the Fourier case are now absent from the EMD analysis. This is because the longer periods are accounted for by the residuals (see Figure 4f). The big dispersion of the energy around periods of 6 years makes it difficult to identify conclusively a geomagnetic oscillation that could directly be related to the changes in dLOD/dt. The dispersion observed might be due to contamination from the 2–3 year periods which, we recall, may well be an artifact of the CHAOS-3 model. Nevertheless, a large number of observatories register signals with a period between 5 and 8 years, as was the case for CM4.

5.3. Spatial Features

[30] Following the suggestion of the previous section that a significant part of the signal of CHAOS-3 has periods between 5 and 8 years, we filtered the SA from this model to that particular band. As done for the Fourier analysis, we detrend, correct and pad the data with zeros before transforming to spectral space. Figure 6 shows maps of $\ddot{B}_r$ at the CMB, filtered to the period range 5–8 years between 2000.6 and 2009.6. Notice that even though signals could have any periodicity within the 5 to 8 year bracket, the strongest features cycle in periods of roughly 6 years.

[31] The 6 year periodic signal seems to be composed of two main effects. In the Eastern hemisphere, flux patches of different sign seem to originate at high latitudes and migrate to the equatorial region where they then circle each other. At high latitudes, these patches are well correlated with strong patches in the field and the flow accelerations computed by *Silva and Hulot* [2012]. The changes happening below India correlate remarkably well with the pattern of both the 2003 (see, e.g., Figure 9 of *Olsen and Mandea* [2007] or Figures 2 and 3 of *Olsen and Mandea* [2008]) and 2007 [see, e.g., *Chulliat et al.*, 2010] geomagnetic jerks. In the Atlantic hemisphere another two flux patches oscillate between positive and negative sign, again strongly resembling the variations suggested by *Olsen and Mandea* [2008]. We argue that this resemblance is not a coincidence. The 2003 and 2007 events could well be a consequence of the 6 year geomagnetic oscillation at a time when the long-term secular variation is nearly constant (as is the case for most observatories over the last decade) and carry the signature of the associated dLOD/dt.

6. Conclusions

[32] We have looked at the secular acceleration of Earth's main magnetic field between 1997 and 2010 using CHAOS-3 and between 1960 and 2002.5 using CM4. We did this with the goal of identifying and characterizing a 6 year geomagnetic signal brought forth by *Gillet et al.* [2010], which can be related to the periodic changes in the observed LOD [*Mound and Buffett*, 2006, 2007].

[33] Our results show the existence of a 6 year periodic signal in both CM4 and CHAOS-3, although the identification is considerably less robust for the latter. For an SA signal to bear a relation to dLOD/dt it must be the result of interactions of the field with the toroidal zonal flow acceleration at the top of the core, specifically its $\dot{t}_1^{0c}$ and $\dot{t}_3^{0c}$ terms. The magnetic signal generated by such interactions should, furthermore, be nonzonal. We verify that this is the case. The 6 year periodic magnetic signal is found to be dominated by spherical harmonics of order 1 and of degree 1 and 3 and relate to interactions with the flow acceleration of those degrees, respectively.

[34] The spatial features of the 6 year cycle were estimated by filtering of the CHAOS-3 SA. The dominant patches are constrained to the latitudinal band within 30° of the equator and mostly localized under the Atlantic and Indian Oceans. These patches correlate well with recent estimates of the geometry of the 2003 and 2007 geomagnetic jerks [*Olsen and Mandea*, 2007, 2008; *Chulliat et al.*, 2010] and of the changes in flow acceleration related to them [*Silva and*

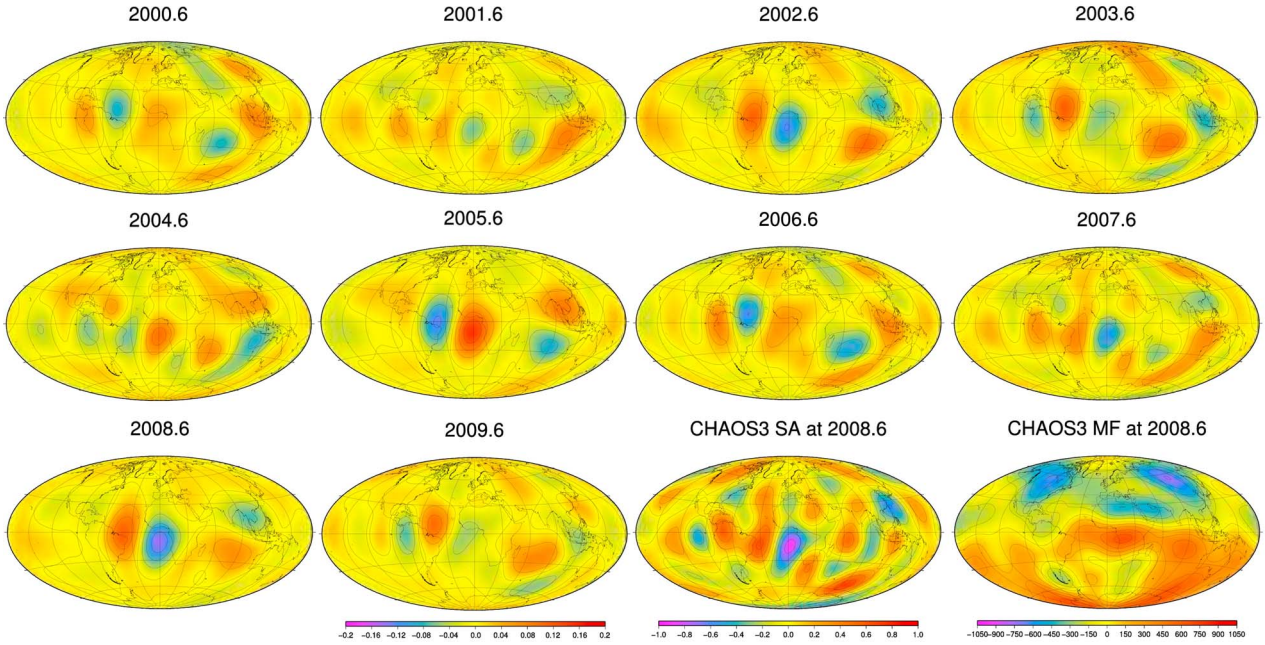

Figure 6. Sequence of maps of filtered $\ddot{B}_r$ at the CMB. The last two maps show the $\ddot{B}_r$ and B_r main field at epoch 2008.6 as provided by CHAOS-3 for comparison. All the maps of SA were truncated to degree and order 8. The map of the main field is truncated at degree and order 13. The map of the main field is in units of μT. The map of the CHAOS-3 SA at 2008.6 is in units of $\mu T/yr^2$. The scale for the filtered SA is given below the 2009.6 map.

Hulot, 2012]. The pattern also seems to be close to that presented by *Le Huy et al.* [1998] for the 1969, 1979 and 1992 geomagnetic jerks. If such a correlation is confirmed for further geomagnetic jerks, the spatial and temporal features of the 6 year cycle described in this paper could be used to improve predictions of the evolution of the geomagnetic secular variation such as the ones used in IGRF [*Finlay et al.*, 2010].

[35] Our results also show that a 2.5 year periodic signal exists in CHAOS-3 and that it is clearly separated from the remaining oscillatory components of the SA. However, we find that both on theoretical and observational grounds, it bears no relation to LOD. The source for this signal still needs to be determined but the possibilities include external sources wrongly mapped onto the internal field, induced sources in the mantle or even an unmodeled oceanic or induced crustal contribution.

[36] **Acknowledgments.** This work was funded by the Natural Environment Research Council (grants NE/G002223/1 and NE/H524673/1). Maps were produced using GMT [*Wessel and Smith*, 1998].

References

Abarca del Rio, R., D. Gambis, and D. A. Salstein (2000), Interannual signals in length of day and atmospheric angular momentum, *Ann. Geophys.*, *18*, 347–364, doi:10.1007/s00585-000-0347-9.

Abramowitz, M., and I. A. Stegun (1964), *Handbook of Mathematical Functions With Formulas, Graphs, and Mathematical Tables*, *Appl. Math. Ser.*, vol. 55, Natl. Bur. of Stand., Washington, D. C.

Chulliat, A., and G. Hulot (2000), Local computation of the geostrophic pressure at the top of the core, *Phys. Earth Planet. Inter.*, *117*, 309–328, doi:10.1016/S0031-9201(99)00104-1.

Chulliat, A., E. Thébault, and G. Hulot (2010), Core field acceleration pulse as a common cause of the 2003 and 2007 geomagnetic jerks, *Geophys. Res. Lett.*, *37*, L07301, doi:10.1029/2009GL042019.

Finlay, C. C., et al. (2010), International geomagnetic reference field: The eleventh generation, *Geophys. J. Int.*, *183*, 1216–1230, doi:10.1111/j.1365-246X.2010.04804.x.

Gibert, D., and J.-L. Le Mouël (2008), Inversion of polar motion data: Chandler wobble, phase jumps, and geomagnetic jerks, *J. Geophys. Res.*, *113*, B10405, doi:10.1029/2008JB005700.

Gillet, N., D. Jault, E. Canet, and A. Fournier (2010), Fast torsional waves and strong magnetic field within the Earth's core, *Nature*, *465*, 74–77, doi:10.1038/nature09010.

Greff-Lefftz, M., and H. Legros (1995), Core-mantle coupling and polar motion, *Phys. Earth Planet. Int.*, *91*, 273–283, doi:10.1016/0031-9201(95)03025-R.

Hide, R., D. H. Boggs, J. O. Dickey, D. Dong, R. S. Gross, and A. Jackson (1996), Topographic core-mantle coupling and polar motion on decadal time-scales, *Geophys. J. Int.*, *125*, 599–607, doi:10.1111/j.1365-246X.1996.tb00022.x.

Hinderer, J., H. Legros, C. Gire, and J.-L. Le Mouël (1987), Geomagnetic secular variation, core motions and implications for the Earth's wobbles, *Phys. Earth Planet. Inter.*, *49*, 121–132, doi:10.1016/0031-9201(87)90136-1.

Hinderer, J., H. Legros, D. Jault, and J.-L. Le Mouël (1990), Core-mantle topographic torque: A spherical harmonic approach and implications for the excitation of the Earth's rotation by core motions, *Phys. Earth Planet. Inter.*, *59*, 329–341, doi:10.1016/0031-9201(90)90237-R.

Holme, R. (2010), Localising the effects of geomagnetic jerks in length-of-day, paper presented at 12th Symposium of SEDI, Study of the Earth's Deep Inter., Santa Barbara, Calif.

Holme, R., and O. De Viron (2005), Geomagnetic jerks and a high resolution length-of-day profile for core studies, *Geophys. J. Int.*, *160*, 435–439, doi:10.1111/j.1365-246X.2004.02510.x.

Holme, R., N. Olsen, and F. L. Bairstow (2011), Mapping geomagnetic secular variation at the core-mantle boundary, *Geophys. J. Int.*, *186*(2), 521–528, doi:10.1111/j.1365-246X.2011.05066.x.

Huang, N., and Z. Wu (2008), A review on Hilbert-Huang transform: Method and its applications to geophysical studies, *Rev. Geophys.*, *46*, RG2006, doi:10.1029/2007RG000228.

Huang, N., et al. (1998), The empirical mode decomposition and the Hilbert spectrum for nonlinear and non-stationary time series analysis, *Proc. R. Soc. London, Ser. A*, *454*, 903–995, doi:10.1098/rspa.1998.0193.

Hulot, G., J.-L. Le Mouël, and J. Wahr (1992), Taking into account truncation problems and geomagnetic model accuracy in assessing computed flows at the core-mantle boundary, *Geophys. J. Int.*, *108*, 224–246, doi:10.1111/j.1365-246X.1992.tb00852.x.

Hulot, G., M. Le Huy, and J.-L. Le Mouël (1996), Influence of core flows on the decade variations of the polar motion, *Geophys. Astrophys. Fluid Dyn.*, *82*, 35–67, doi:10.1080/03091929608213629.

Jackson, A., J. Bloxham, and D. Gubbins (1993), Time-dependent flow at the core surface and conservation of angular momentum in the coupled core-mantle system, in *Dynamics of Earth's Deep Interior and Earth Rotation*, *Geophys. Monogr. Ser.*, vol. 72, pp. 97–107, AGU, Washington, D. C.

Jackson, L. P., and J. Mound (2010), Geomagnetic variation on decadal time scales: What can we learn from empirical mode decomposition?, *Geophys. Res. Lett.*, *37*, L14307, doi:10.1029/2010GL043455.

Jault, D., and J. Le Mouël (1991), Exchange of angular momentum between the core and the mantle, *J. Geomagn. Geoelectr.*, *43*(2), 111–129.

Jault, D., C. Gire, and J.-L. Le Mouël (1988), Westward drift, core motions and exchanges of angular momentum between core and mantle, *Nature*, *333*(6171), 353–356, doi:10.1038/333353a0.

Ladynin, A. V., and A. A. Popova (2008), Quasi-periodic geomagnetic secular variation (from 1985–2005 world observatory data), *Russ. Geol. Geophys.*, *49*, 951–962, doi:10.1016/j.rgg.2008.04.006.

Le Huy, M., M. Alexandrescu, G. Hulot, and J.-L. Le Mouël (1998), On the characteristics of successive geomagnetic jerks, *Earth Planets Space*, *50*, 723–732.

Lesur, V., I. Wardinski, M. Hamoudi, and M. Rother (2010), The second generation of the GFZ Reference Internal Magnetic Model: GRIMM-2, *Earth Planets Space*, *62*, 765–773, doi:10.5047/eps.2010.07.007.

Maus, S., L. Silva, and G. Hulot (2008), Can core-surface flow models be used to improve the forecast of the Earth's main magnetic field?, *J. Geophys. Res.*, *113*, B08102, doi:10.1029/2007JB005199.

McLeod, M. G. (1996), Spatial and temporal power spectra of the geomagnetic field, *J. Geophys. Res.*, *101*(B2), 2745–2763, doi:10.1029/95JB03042.

Mound, J., and B. Buffett (2006), Detection of a gravitational oscillation in length-of-day, *Earth Planet. Sci. Lett.*, *243*, 383–389, doi:10.1016/j.epsl.2006.01.043.

Mound, J., and B. Buffett (2007), Viscosity of the Earth's fluid core and torsional oscillations, *J. Geophys. Res.*, *112*, B05402, doi:10.1029/2006JB004426.

Olsen, N., and M. Mandea (2007), Investigation of a secular variation impulse using satellite data: The 2003 geomagnetic jerk, *Earth Planet. Sci. Lett.*, *255*, 94–105, doi:10.1016/j.epsl.2006.12.008.

Olsen, N., and M. Mandea (2008), Rapidly changing flows in the Earth's core, *Nat. Geosci.*, *1*, 390–394, doi:10.1038/ngeo203.

Olsen, N., M. Mandea, T. Sabaka, and L. Tøffner-Clausen (2010), The CHAOS-3 geomagnetic field model and candidates for IGRF-2010, *Earth Planets Space*, *62*, 719–727, doi:10.5047/eps.2010.07.003.

Ponsar, S., V. Dehant, R. Holme, D. Jault, M. A. Pais, and T. Van Hoolst (2003), The core and fluctuations in the Earth's rotation, in *Earth's Core: Dynamics, Structure, Rotation*, *Geodyn. Ser.*, vol. 31, pp. 261–261, AGU, Washington, D. C.

Roberts, P. H., Z. Yu, and C. Russell (2007), On the 60-year signal from the core, *Geophys. Astrophys. Fluid Dyn.*, *101*(1), 11–35, doi:10.1080/03091920601083820.

Sabaka, T., N. Olsen, and M. Purucker (2004), Extending comprehensive models of the Earth's magnetic field with Ørsted and CHAMP data, *Geophys. J. Int.*, *159*, 521–547, doi:10.1111/j.1365-246X.2004.02421.x.

Silva, L., and G. Hulot (2012), Investigating the 2003 geomagnetic jerk by simultaneous inversion of the secular variation and acceleration for both the core flow and its acceleration, *Phys. Earth Planet. Inter.*, *198-199*, 28–50, doi:10.1016/j.pepi.2012.03.002.

Wardinski, I. (2005), Core surface flow models from decadal and subdecadal secular variation of the main geomagnetic field, Ph.D. thesis, Dtsch, GeoForschungsZentrum, Potsdam, Germany.

Wessel, P., and W. H. F. Smith (1998), New, improved version of the generic mapping tools released, *Eos Trans. AGU*, *79*, 579.